International Journal of Control and Automation
Vol.8, No.11 (2015), pp.225-234
http://dx.doi.org/10.14257/ijca.2015.8.11.22

Numerical Investigation of a Pumpjet Propulsor Based on CFD

Guang Pan[1] and Lin Lu[1]

[1]*School of Marine Science and Technology, Institute of Underwater Vehicle, Northwestern Polytechnical University, Xi'an, 710072, China; luluhenry1234@163.com*

Abstract

In this study an attempt has been made to study the hydrodynamic performance of pumpjet propulsor. Numerical investigation based on the Reynolds Averaged Navier-Stokes (RANS) computational fluid dynamics (CFD) method using structured grid, SST k-ω turbulence model has been carried out. The grid independence inspection is applied to verify accuracy of numerical simulation. The numerical predictions of hydrodynamic performance for pumpjet propulsor are carried out with different advance ratios. Results show that the coefficient curves of thrust and torque that indicates the rotor provides the main thrust of propulsor and the balance performance of propulsor is generally satisfactory. Additionally, the curve of propulsor efficiency is in good agreement with experimental data. Furthermore, the pressure distributions around rotor and stator blades are reasonable. Beyond that, the existence of tip clearance accounts for the appearance of tip vortex that leads to a further loss in efficiency and a probability of cavitation phenomenon. .

Keywords: *Pumpjet propulsor, numerical investigation, hydrodynamic performance, computational fluid dynamic*

1. Introduction

With the last decade, numerous numerical and experimental researches for the water jet propulsion, axial-flow pump and centrifugal pump were carried out and some useful results about the velocity, pressure and hydraulic loss have been achieved. Park presented the numerical analysis of a waterjet propulsion system to provide a detailed understanding of complicated three-dimensional viscous flow phenomena. The complicated viscous flow feature of the waterjet are well understood by the present simulation. The performances of thrust and torque are also predicted [1]. Li Y and Wang F carried out a numerical investigation on an axial-flow pump equipped with an inducer. The pump performances are predicted and compared to the experimental measurements. Recommendations for future modifications and improvements to the pump design are also given [2]. Gao investigated the performance and three-dimensional flow fields in a water-jet pump. Overall performances as predicted by CFD simulation are in good agreement with the experimental results. In addition, the effects of a rear stator and different spacing between the rotor and the stator on the overall performance and the flow fields of the water-jet pump have also been investigated [3]. Zhang simulated the three-dimensional unsteady turbulent flow in axial-flow pumps based on Navier-Stokes solver embedded with k-ε RNG turbulence model and SIMPLEC algorithm. Numerical results show that the unsteady prediction results are more accurate than the steady results, and the maximum error encountered in unsteady prediction is only 4.54% [4]. Petit applied CFD analyses to study the unsteady three-dimensional turbulence in the ERCOFTAC centrifugal pump test case using the OpenFOAM software. Results of steady and unsteady calculations of the flow in the pump are compared with the experimental ones. The comparisons show that the unsteady numerical results accurately predict the unsteadiness [5]. Their researches

ISSN: 2005-4297 IJCA

play an important role for further research of numerical simulation of pumpjet propulsor. However, present literature review suggests that the numerical simulation of hydrodynamic performance for pumpjet propulsor is few and far between. Though experimental studies of hydrodynamic performance can accurately reflect the variation of the flow field, experiments are time-consuming and cannot be carried out for some complex operating conditions. With the rapid development of computational methods, CFD has become more and more practical and been widely used in the studies of 3-D turbulent flows. Ivanell described a CFD model of the pumpjet propulsor on a torpedo using FLUENT to verify its accuracy by comparing numerical simulation results with wind tunnel experiments. It can be concluded from the simulations that the results for the propulsion force is about 10% higher when compared with the measurements. The result for the resistance force is about 17% higher [6]. Suryanarayana evaluated open water hydrodynamics and cavitation performance of the pumpjet propulsor on an axi-symmetric underwater body through CFD study [7-8]. Their investigative efforts show that the stator can absorb the rotational energy of the rotor and reduce the radial component of wake flows leading to the increase of propulsor efficiency.

In this study, three-dimensional rotor-stator coupling flow fields in a pumpjet propulsor are investigated using the *SST k–ω* turbulence model and finite volume method based on the RANS method. The grid independence inspection is verified, and the CFD-predicted overall hydrodynamic performances for pumpjet propulsor are compared with experimental results. In addition, the pressure distribution of rotor and stator blades are also studied at the same time.

2. Numerical Simulation Method

2.1. Governing Equations

The governing equations for the turbulent incompressible flow encountered in this research are the three-dimensional RANS equations for the conservation of mass and momentum, given as:

$$\frac{\partial}{\partial x_i}(\rho \bar{u}_i) = 0 \tag{1}$$

$$\frac{\partial}{\partial t}(\rho \bar{u}_i) + \frac{\partial}{\partial x_j}(\rho \bar{u}_i \bar{u}_j) = \rho \bar{F}_i - \frac{\partial \bar{p}}{\partial x_i} + \frac{\partial}{\partial x_j}\left[\mu\left(\frac{\partial \bar{u}_i}{\partial x_j} + \frac{\partial \bar{u}_j}{\partial x_i}\right)\right] \tag{2}$$

where $\bar{p}$ is the average pressure, μ is the molecular viscosity and $\rho \bar{u}_i \bar{u}_j$ is the Reynolds stress. To correctly account for turbulence, the Reynolds stresses are modeled in order to achieve the closure of equation (2). The Boussinesq approximation leads to the use of an eddy viscosity μ_t to model the turbulent Reynolds stresses.

$$-\rho \overline{u_i' u_j'} = \mu_t\left(\frac{\partial \bar{u}_i}{\partial x_j} + \frac{\partial \bar{u}_j}{\partial x_i}\right) - \frac{2}{3}\delta_{ij} \bullet \left(\rho k + \mu_t \frac{\partial \bar{u}_i}{\partial x_i}\right) \tag{3}$$

where μ_t is the turbulent viscosity and k is the turbulent kinetic energy.

2.2. Turbulence Model

According to the existing study by Ji.[9], the *SST k–ω* turbulence model is applied for closing the numerical simulation in this study. The *SST k–ω* turbulence model combines the advantages of stability of the near-wall k–ω turbulence model

and independent of the external boundary k–ε turbulence model. The *SST* k–ω turbulence model has the following advantages specifically: it can adapt to a variety of physical phenomenon caused by the pressure gradient changes, and it can utilize the inner viscous layer combined with the wall function to accurately simulate the phenomenon of the boundary layer without the use of easier distortion viscous-attenuation function. When calculating, the solving program based on Reynolds number automatically invokes different turbulence models. In the low Reynolds number regions, the k–ω turbulence model is applied. In the high Reynolds number regions, the k–ε turbulence model is adopted. Consequently, the *SST* k–ω turbulence model has better applicability in dealing with boundary problems of different Reynolds numbers.

3. Computational Model and Grid

3.1. Model Geometry and Computational Domain

In this study, the whole hydraulic passage of the pumpjet propulsor is selected as the computational geometry of numerical simulation as shown in Figure 1. The diameter of pumpjet propulsor is Dt=0.324m. This pumpjet propulsor has 11 rotor blades, 9 stator blades, and the minimum clearance size between the rotor blade tip and the duct is 1*mm*.

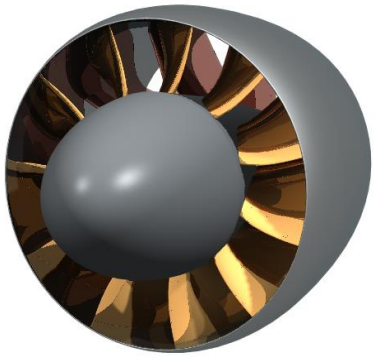

Figure 1. Pumpjet Propulsor Computational Geometry

The computational domain and boundary conditions are shown as Figure 2. The computational domain is a length of 11Dt, diameter of 10Dt cylinder surrounding the pumpjet propulsor, whose axis coincides with the symmetry axis. The inlet is located 4Dt from the front face of pumpjet propulsor, and the outlet is situated 6Dt from the end of propulsor. According to the structural characteristics of the pumpjet propulsor, the computational domain is divided into three parts: rotor domain, stator domain and external flow field domain. The rotor domain is a rotating domain, the other two domains are stationary domains. The rotor and stator domains are embedded in the external flow field domain. The interactions between the rotor domain and stator domain are solved by using the sliding mesh method.

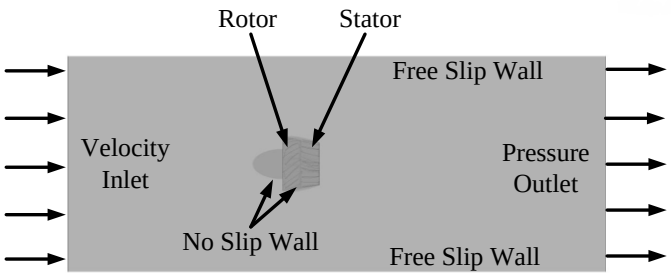

Figure 2. Computational Domain and Boundary Conditions for Pumpjet Propulsor

3.2. Grid Generation

The quality of computational grid directly affects the convergence and results of numerical analysis. The structured grid has the advantage of using less memory and is very favorable for the boundary layer calculation. Therefore, all the computational domains are filled with structured grids generated by ANSYS ICEM. According to the division of the computational domain, multi-block grid method is selected to generate high-quality structured grid. The grids around pumpjet propulsor adopt H hybrid grids. The propulsor blade surface is surrounded by O-hexahedral girds. The number of entire computational domain grids is approximately 1.5×10^6, including 7×10^5 rotor domain grids and 4.5×10^5 stator domain girds. Figure 3 and Figure 4 show the computational domain girds of the external flow field and the rotor and stator blades surface grids, respectively. Three interfaces between the rotor, the stator and the external flow field are formed, as shown in Figure 3.

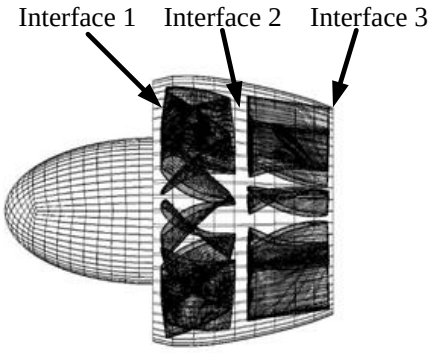

Figure 3. Surface Grids of Pumpjet Propulsor

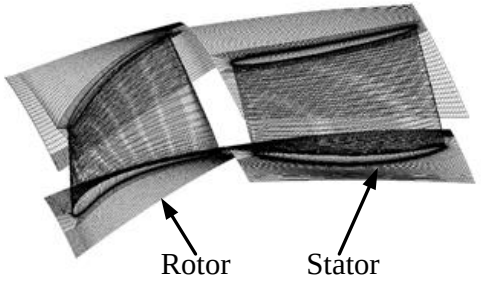

Figure 4. Surface Grids of the Rotor and Stator Blades

3.3. Boundary Condition

The setting of boundary condition plays a direct influence on the completion of numerical simulation. For computational domain boundary conditions, the inlet boundary is set to normal speed, turbulence intensity is 5% as the default. The no-slip boundary condition is imposed on duct and blades. The free-slip wall boundary is imposed on the cylinder surface. The averaged static pressure is specified at the outlet. The interface between the rotor domain and stator domain is set to frozen rotor. The time derivatives are calculated using a second-order backward Euler algorithm, the spatial derivatives are calculated using a second-order upwind algorithm, and the finite volume method is selected for the discretization of equation. (3).

4. Results and Discussion

In the following sections, the advance ratio J is defined, as $J = U_\infty / (nD)$, where U_∞ denotes the free stream velocity, n is the blade rotational velocity. In addition, maintain U_∞ equal to $25.72 m s^{-1}$ and change n from 1500rps to 4000rps to obtain different advance ratios. The thrust coefficients of rotor and stator are defined as $K_{T_r} = T_r / (\rho_f n^2 D^4)$ and $K_{T_s} = T_s / (\rho_f n^2 D^4)$. The torque coefficients of rotor and stator are defined as $K_{Q_r} = Q_r / (\rho_f n^2 D^5)$ and $K_{Q_s} = Q_s / (\rho_f n^2 D^5)$, where T_r and T_s represent the thrust of rotor and stator, respectively. Q_r and Q_s denote the torque of thrust of rotor and stator, respectively. The thrust coefficient and torque coefficient of pumpjet propulsor are defined as $K_T = T_r + T_s$ and $K_Q = Q_r$, respectively. The pumpjet propulsor efficiency $\eta = (J \times K_T)/(2\pi \times K_Q)$ is defined.

4.1. Grid Independent Inspection

The gird independent inspection is applied in order to ensure the accuracy and precision of numerical simulation. The computational grid is regenerated by reducing the size of the first layer of wall grids. Table 1 shows the numerical results of hydrodynamic performance of propulsor with three different advance ratios, J=1.69, 2.24, 3.01. As shown in Table 1, the errors of different coefficients are less than 1% after the girds are refined, and the gird independence has been verified. However, the refined grid results in an increase in simulation time and a decline in grid quality. Consequently, the undefined grid has been selected for numerical simulation and analysis.

Table 1. Numerical Simulation Results of Unrefined and Refined Grids with Different Advance Ratios

J		K_{T_r}	K_{T_s}	K_{Q_r}	K_{Q_s}
1.69	Unrefined	1.1753	0.2762	0.4425	0.4457
	Refined	1.1731	0.2743	0.4397	0.4432
2.24	Unrefined	0.8591	0.1264	0.3903	0.4038
	Refined	0.8565	0.1221	0.3868	0.4002
3.01	Unrefined	0.0324	-0.2492	0.2392	0.2402
	Refined	0.0301	-0.2469	0.2358	0.2373

4.2. Cfd Results and Discussion

The numerical invest igation and experimental results of propulsor efficiency curves are shown in Figure 5. As can be seen from Figure 5, the pumpjet propulsor efficiency increases with the increasing of advance ratio and then decreases, and achieves the maximum at J=2.51. The numerical simulation results are in agreement with experimental data reported by Liu [10]. However, the results of numerical simulation are slightly larger than those of experiment. That is mainly because the circumstance of numerical simulation sets more idealistic. The results of CFD calculation and experimental work show reasonably good correlation. Hence it may be presumed that CFD modelling has been carried out with a reasonable degree of accuracy and confidence.

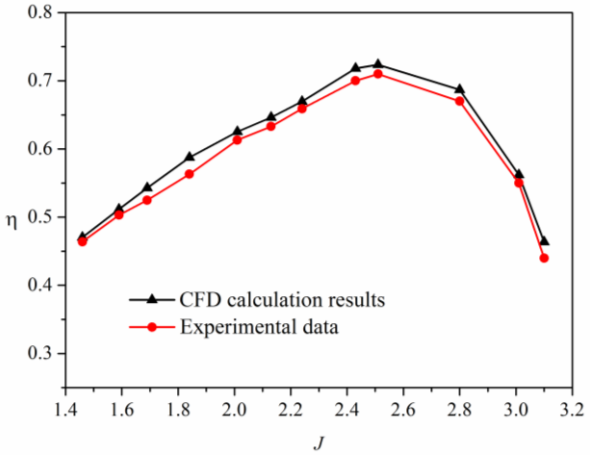

Figure 5. Pumpjet Propulsor Efficiency Curves with Different Advance Ratios

The results of numerical simulation of pumpjet hydrodynamic performance are summarized in Table 2. According to the results in Table 1, the pumpjet hydrodynamic performance curves are shown in Figure 6. As can be seen from Figure 6, the thrust of rotor is much larger than that of stator as J is relative small, which indicates that the main thrust of pumpjet propulsor is derived from the rotor. The thrust of stator has a good linear relation with the J. In addition, the thrust of stator changes into resistance as J is larger than 2.43, which accounts for the loss of propulsor efficiency. That is coincident with the efficiency curve in Figure 5. According to the trend of curves, the thrust and torque of the rotor and stator decrease with the increase of the advance ratio. Furthermore, there is almost no difference between the torque of rotor and stator. The errors is less than 8%, which demonstrates that the balance performance of pumpjet propulsor is generally satisfactory.

Table 2. Numerical Simulation Results of Hydrodynamic Performance of Pumpjet Propulsor

J	K_{T_r}	K_{T_s}	K_{Q_r}	K_{Q_s}
1.46	1.2582	0.3459	0.4509	0.4509
1.59	1.2129	0.3071	0.4464	0.4482
1.69	1.1753	0.2762	0.4425	0.4457
1.84	1.1022	0.2242	0.4321	0.4379
2.01	1.0087	0.1626	0.4175	0.4263

2.13	0.9322	0.1264	0.4039	0.4151
2.24	0.8591	0.1166	0.3903	0.4038
2.43	0.6847	-0.0053	0.3524	0.3717
2.51	0.6209	-0.0346	0.3402	0.3620
2.80	0.3136	-0.1540	0.2715	0.3034
3.01	0.0324	-0.2492	0.2208	0.2402

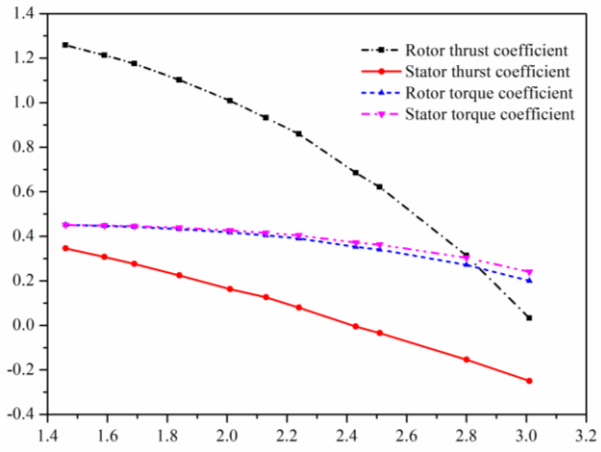

Figure 6. Pumpjet Propulsor Hydrodynamic Performance Curves

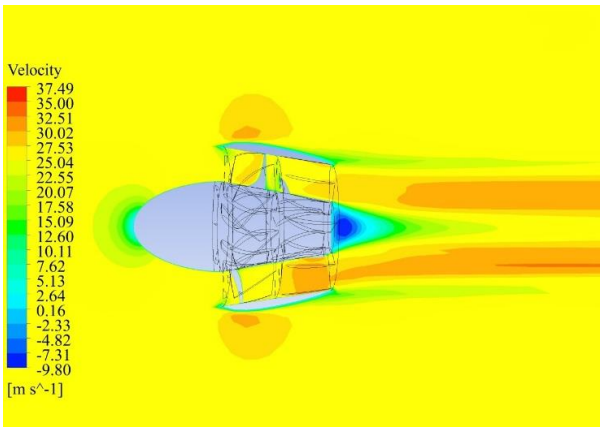

Figure 7. Velocity Distribution of the Axial Cross Section of the Pumpjet Propulsor

Figure 7 shows the velocity distribution of the axial cross section of the pumpjet propulsor at J=2.38. From Figure 7 we can see, the flow has been obviously accelerated after it goes through the rotor and stator blades, which suggests that the stator increases the thrust of propulsor and then accelerate the coming flow. Beyond that, there is a greater velocity in the clearance between the rotor blade tip and duct, which probably results in the occurrence of cavitation phenomenon in this blade region.

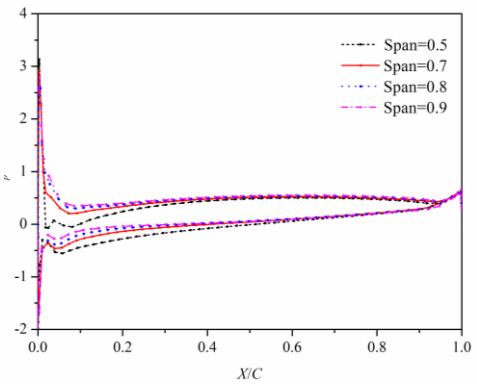

Figure 8. Pressure Coefficient Distribution Of Rotor Blade Along Blade Chord Direction With Different Spans

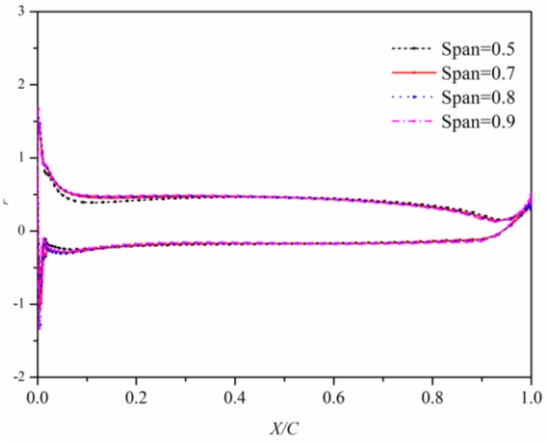

Figure 9. Pressure Coefficient Distribution of Stator Blade along Blade Chord Direction with Different Spans

Figures 8 and 9 show the curves of the pressure coefficients, defined as $C_p = (p - p_{out}) / 0.5\rho_f U_\infty{}^2$, of rotor and stator blades, respectively, which represent the pressure distribution along the blade chord direction at J=2.23 with different span. X denotes the distance from monitoring pressure point to the leading edge and C represents the chord length, where p is the local pressure, p_{out} is the outlet pressure. Due to the existence of the duct, the inlet velocity of propulsion has been reduced significantly, so that the rotor and stator can work in a relative high pressure environment which can delay the inception of cavitation and reduce the noise. In addition, there is a great pressure gradient at the leading edge of the pressure side of the rotor and stator blades as shown in Figure 8 and Figure 9. In the middle of the blade surface, the pressure coefficients of the pressure side of the rotor and stator blades remain nearly constant. Furthermore, the pressure around the leading edge of rotor suction side is relatively low, which may cause the appearance of cavitation phenomenon. Simultaneously, there is a small clearance between the rotor blade tip and duct for pumpjet propulsor, so that the pressure of pressure side of the rotor blade is higher than that of suction side, which finally accounts for the back-flow and the probability of emergence of tip vortex that are unfavorable factors for propulsion efficiency.

5. Conclusions

In this study, numerical investigation and analysis of steady flows around pumpjet propulsor have been presented. A constructed grid based on RANS is applied. The *SST k–ω* turbulence model and finite volume method have been employed. The hydrodynamic performance of pumpjet propulsor has been investigated.

The grid independence inspection was applied with three different advance ratios to verify accuracy and precision of numerical simulation. The results show that the errors are less than 1% after the girds are refined. However, the refined grid results in an increase in simulation time and a decline in grid quality. Consequently, the undefined grid has been selected for numerical simulation and analysis.

The computational results in CFD of pumpjet propulsor efficiency and experimental data shows reasonably good correlation. The computed results indicate that the efficiency of pumpjet propulsor increases with the increasing of J and then decrease, and achieves the maximum at J=2.51. In addition, the results of numerical simulation are slightly larger than those of experiment because of the idealistic sets of numerical investigation.

Numerical investigation of pumpjet hydrodynamic performance has been presented and summarized. The thrust of rotor is much larger than that of stator, which indicates that the rotor provides the main thrust of pumpjet propulsor. Furthermore, there is basically no difference between the torque of rotor and stator. The errors is less than 8%, which demonstrates that the balance performance of pumpjet propulsor is generally satisfactory. The velocity distribution of the axial cross section of the pumpjet propulsor shows that the flow has been obviously accelerated after it goes through the rotor and stator blades, which demonstrates that the stator increases the thrust of propulsor and then accelerate the coming flow.

The pressure distributions of the rotor and stator blades show that the pressure around the leading edge of rotor suction side is relatively low, which may cause the appearance of cavitation phenomenon. Simultaneously, there is a small clearance between the rotor blade tip and duct, so that the pressure of pressure side of the rotor blade is higher than that of suction side, which finally accounts for the back-flow and the emergence of tip vortex that are unfavorable for propulsion.

Acknowledgements

This work was supported by the National Natural Science Foundation of China [Grant No.51479170].

References

[1] W. Park, JH. Jang, HH. Chun and CM. Kim, “Numerical flow and performance analysis of waterjet propulsion system”, Ocean Engineering, vol. 32, no. 14-15, **(2005)**, pp. 1740-1761.
[2] Y. Li and F. Wang, “Numerical investigation of performance of an axial-flow pump with inducer”, Journal of Hydrodynamics, vol. 19, no. 6, **(2007)**, pp. 705-711.
[3] H. Gao, W. Lin and Z. Du, “Numerical flow and performance analysis of a water-jet axial flow pump”, Ocean Engineering, vol. 35, no. 16, **(2008)**, pp. 1604-1614.
[4] D. Zhang, W. Shi, B. Chen and X. Guan, “Unsteady flow analysis and experimental investigation of axial-flow pump”, Journal of Hydrodynamics, vol. 22, no. 1, **(2010)**, pp. 35-43.
[5] O. Petit and H. Nilsson, “Numerical investigations of unsteady flow in a centrifugal pump with a vaned diffuser”, International Journal of Rotating Machinery, vol. 2013, no. 1, **(2013)**, pp. 1-14.
[6] S. Ivanell, “Hydrodynamic simulation of a torpedo with pump jet propulsion system”, Master Thesis, Royal Institute of Technology, Stockholm, Sweden, **(2001)**, 77pp.
[7] Ch. Suryanarayana, B. Satyanarayana, K. Ramji and A. Saiju, “Experimental evaluation of pumpjet propulsor for an axisymmetric body in wind tunnel”, International Journal of Naval Architecture and Ocean Engineering, vol. 2, no. 1, **(2010)**, pp. 24-33.

[8] Ch. Suryanarayana, B. Satyanarayana, K. Ramji and A. Saiju, "Experimental evaluation of pumpjet propulsor for an axisymmetric body in wind tunnel", International Journal of Naval Architecture and Ocean Engineering, vol. 2, no. 1, **(2010)**, pp. 57-67.
[9] B. Ji, X. Luo, Y. Wu, S. Liu and A. Oshima, "Numerical investigation of unsteady cavitating turbulent flow around a full scale marine propeller", Journal of Hydrodynamics, vol. 22, no. 5, **(2010)**, pp. 747-752.
[10] Z. Liu, B. Song, Q. Huang and H. Hu, "Applying CFD technique to calculating successfully hydrodynamic performance of water jet pump", Journal of Northwestern Polytechnical University, vol. 28, no. 5, **(2010)**, pp. 724-729.

Authors

Guang Pan, male, he was born on March, 1969, ethnic Han. He is the Northwestern Polytechnical University professor, doctoral supervisor. His main research interests focus on the overall UUV technology, fluid dynamics, underwater trajectory MDO.

Lin Lu, male, he was born on July, 1988. He is a PhD candidate of School of Marine Science and Technology, Northwestern Polytechnical University. His main research interests include propulsion design, hydrodynamic performance, numerical simulation and cavitation investigation for different propulsors.

